Environmental Science & Technology

pubs.acs.org/est

Article

Plutonium Redox Transformation in the Presence of Iron, Organic Matter, and Hydroxyl Radicals: Kinetics and Mechanistic Insights

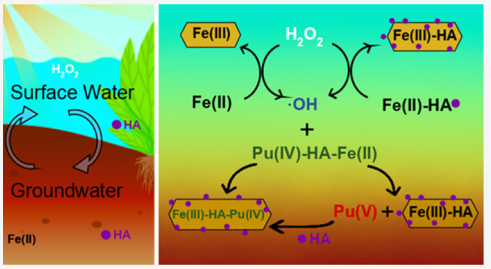
Chao Pan,* Yongqin Jiao, Annie B. Kersting, and Mavrik Zavarin

Cite This: *Environ. Sci. Technol.* 2021, 55, 1800−1810

Read Online

ACCESS | Metrics & More | Article Recommendations | Supporting Information

ABSTRACT: Plutonium (Pu) redox and complexation processes in the presence of natural organic matter and associated iron can impact the fate and transport of Pu in the environment. We studied the fate of Pu(IV) in the presence of humic acid (HA) and Fe(II) upon reaction with H_2O_2 that may be generated by photochemical and other reactions. A portion of Pu(IV) was oxidized to Pu(V/VI), which is primarily ascribed to the generation of reactive intermediates from the oxidation of Fe(II) and Fe(II)−HA complexes by H_2O_2. The kinetics of Pu(IV) oxidation is pH-dependent and can be described by a model that incorporates Pu redox kinetics with published HA-modified Fenton reaction kinetics. At pH 3.5, the presence of HA slowed Pu(IV) oxidation, while at pH 6, HA accelerated Pu(IV) oxidation in the first several hours followed by a reverse process where the oxidized Pu(V/VI) was reduced back to Pu(IV). Analysis of Pu-associated particle size suggests that Pu oxidation state is a major driver in its complexation with HA and formation of colloids and heteroaggregates. Our results revealed the H_2O_2-driven oxidation of Pu(IV)−HA−Fe(II) colloids with implications to the transient mobilization of Pu(V/VI) in organic-rich redox transition zones.



Downloaded via LOS ALAMOS NATL LABORATORY on September 3, 2025 at 22:29:23 (UTC).
See https://pubs.acs.org/sharingguidelines for options on how to legitimately share published articles.

1. INTRODUCTION

Pu contamination of soil and groundwater is a legacy of past activities associated with the production of nuclear weapons (e.g., Hanford Site and Savannah River Site, USA), nuclear weapon tests,[1] as well as the discharge of radionuclides from commercial fuel reprocessing into the environment (e.g., Sellafield, UK).[2−5] The fate and transport of Pu in water is governed by processes that include redox reactions,[6,7] adsorption to and desorption from mineral surfaces,[8−10] dissolution and precipitation,[11] interactions with natural organic matter (NOM),[12,13] and microbial activity which can mediate these geochemical processes and directly impact Pu behavior.[14−17] Under environmental conditions, Pu can exist as Pu(III), Pu(IV), Pu(V), and Pu(VI).[18] Environmental redox processes play a critical role in controlling Pu mobility as the reduced forms (III/IV) are generally 2−3 orders of magnitude less mobile and have higher affinity for mineral surfaces and organic matter than the oxidized forms (V/VI) in most environments.[9,19,20] However, formation of intrinsic Pu(IV) oxide/hydroxide and pseudo Pu colloids could facilitate the subsurface transport of Pu under certain conditions.[21] The presence of these colloids further complicates the fate of Pu as it can lead to mobilization of the reduced forms of Pu via colloid-facilitated transport.[10,22,23]

NOM is ubiquitous in aquatic environments and profoundly impacts the biogeochemical cycling of metals and radionuclides.[24−27] NOM comprises complex heterogeneous organic macromolecules, a fraction of which has been traditionally classified as humic substances. Recently, the traditional classification of humic substances by alkaline extraction has been challenged.[28] Nevertheless, these organic compounds can influence the fate and transport of Pu through redox and complexation reactions.[29] Pu(V/VI) can be rapidly reduced to Pu(III/IV) by NOM, depending on the nature of the organic matter.[30,31] In addition, NOM will complex Pu via carboxylate functionalities and nitrogen groups in both colloidal and particulate phases.[32] Santschi et al. revealed that the majority of the remobilized Pu from contaminated soils to streams in storm runoffs, pond discharge, and wind dispersion events at Rocky Flats National Wildlife Refuge was associated with organic macromolecules rather than the more abundant inorganic colloids (iron oxides and clays).[33] In contrast to enhancing Pu mobility, NOM has also been shown to behave as a sink for Pu in many sedimentary systems. Matkar et al. reported that a significant fraction of Pu was associated with sediment organic matter in the coastal environment of Trombay, India. As a result, Pu became available to bottom-feeding organisms and entered the aquatic food chain.[34]

NOM is commonly found associated with Fe(III) oxides in surface water and groundwater,[35−37] and their interactions can control the speciation and transport of Pu depending on

Received: December 4, 2020
Revised: January 4, 2021
Accepted: January 6, 2021
Published: January 20, 2021



© 2021 American Chemical Society

https://dx.doi.org/10.1021/acs.est.0c08195
Environ. Sci. Technol. 2021, 55, 1800−1810

colloidal properties of NOM−Fe.[12,38,39] For example, under oxic conditions, citric acid, humic acid (HA), and fulvic acid (FA) were found to increase Pu adsorption onto Fe(III) oxides at low pH by forming ternary Pu(IV)−NOM−Fe(III) oxide complexes.[12,38] Furthermore, these NOM−Fe colloids have been shown to serve as geochemical nanocarriers, either facilitating or reducing the overall transport of Pu in surface water depending on their particle transport properties.[22,39−41] Chen et al. studied the mobility of Pu in soil-groundwater suspensions and found that Pu(IV) formed mobile colloids with NOM, while Pu(V) sorbed more readily to prevailing solid clay mineral surfaces.[41] During seasonal mixing events and associated transient redox conditions, transport of NOM−Fe(II) colloids from groundwater to surface water can result in the formation of NOM−Fe(III) oxide colloids and generation of hydroxyl radicals.[42,43]

Hydrogen peroxide (H_2O_2) can be generated via photolysis of NOM or reduced NOM and Fe(II) oxygenation in the absence of light.[44−46] It has been observed up to micromolar concentration levels in surface water including lakes, rivers, seas, and atmospheric water droplets.[47,48] H_2O_2 has been demonstrated to drive Pu(IV) desorption from Fe(III) oxides relevant to environmental conditions by decomposition to hydroxyl radicals.[49] It also has been observed to enhance the reduction of Pu(V) to Pu(IV) in seawater, thus potentially decreasing the mobility of Pu.[7] The reaction of H_2O_2 with Fe(II), referred to as Fenton reaction, is important in groundwater-surface water mixing as it can result in the formation of the hydroxyl radicals under *acidic conditions*; these highly reactive species may induce the oxidation of both NOM and contaminants.[50] The reaction of NOM−Fe(II) complexes with H_2O_2 has been shown to form hydroxyl radicals over *a wider range of pH*.[51] For surface water and groundwater interactions, enhanced Pu migration has been observed at the Savannah River site due to Pu(IV) oxidation to Pu(V) from infiltrating and oxidizing rainwater.[52] However, a quite recent study showed that the presence of NOM significantly limited Pu migration through reduction of Pu(V) and increased Pu sorption to soils.[22] These contrasting observations suggest that our understanding of the impact of NOM on Pu migration in surface and groundwater is incomplete.

The objective of this study was to investigate the redox cycling, complexation, and mobility of Pu in the presence of Fe(II), NOM, and H_2O_2. HA filtered through a 0.45 μm cellulose membrane was selected as a representative NOM in this study. The redox kinetics of Pu(IV) in the presence of Fe(II) and HA was monitored upon H_2O_2 addition, mimicking surface water/groundwater mixing and surface water infiltration transient redox events. Particular attention was directed at evaluating the Pu oxidation states and Pu partitioning between truly dissolved, colloidal, and particulate phases. The study provides insights into Pu redox transformations and extends our fundamental understanding of the transport mechanisms controlling Pu migration in surface water and shallow sediments.

2. MATERIALS AND METHODS

2.1. Materials. All stock solutions and suspensions were prepared with ultrapure water (resistivity >18.2 MΩ cm, Milli-Q, Millipore). The HA, hydrogen peroxide (H_2O_2), *tert*-butanol, 2-(*N*-morpholino)ethanesulfonic acid (MES), and *N*,*N*-diethyl-*p*-phenylenediamine (DPD) were purchased from Sigma-Aldrich. MES did not appear to act as a Pu(V/VI) reductant (Figure 1b, no HA data). Nevertheless, a more detailed study of Pu(VI) reduction by MES should be considered in future studies. The Sigma-Aldrich HA displays similar redox properties as those of soil-derived HAs and has been used in numerous other studies.[26,53] The stock suspension of HA was filtered through 0.45 μm Millipore membrane and stored in the dark at 4 °C prior to use.

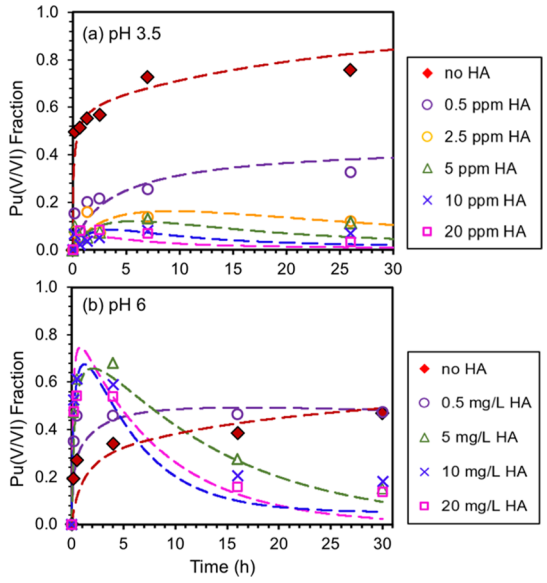


Figure 1. Effect of HA on Pu(IV)−HA−Fe(II) reaction with H_2O_2 at (a) pH 3.5 and (b) pH 6. $Fe(II)_0$ = 100 μM, $Pu(IV)_0$ = 10^{-10} M, H_2O_2 = 100 μM, NaCl = 5 mM, pH 6 experiments were buffered with 0.5 mM MES. The dashed lines represent fitted kinetic modeling results.

A ^{238}Pu stock containing 99.77% ^{238}Pu, 0.16% ^{241}Pu, and 0.04% ^{239}Pu by activity (0.1 μCi/mL) was used to prepare the Pu stock solution. Pu was first reacted with $NaNO_2$ and reduced to Pu(IV). The Pu stock solution was then purified using anion exchange resin (BioRad AG 1 × 8, 100−200 mesh) preconditioned with 8 M HNO_3. The Pu was loaded on the resin in 8 M HNO_3, washed with three column volumes of 8 M HNO_3, and then eluted in 0.1 M HCl.[10,54] The final Pu(IV) concentration in the stock solution was determined to be 8.84 × 10^{-8} M. A Pu(VI) stock was prepared using an electrochemistry method described in previous studies.[14,31] Briefly, the purified Pu(IV) stock was added to an electrochemical cell with 0.1 M $NaNO_3$ electrode solution at 1.9 V for 5 days.

2.2. Batch Experiments. All batch experiments with Pu were conducted at room temperature (22 ± 1 °C) using 15 mL Nalgene Oak Ridge polycarbonate centrifuge tubes and set on a shaker table at 125 rpm. The tubes were shielded with aluminum foil to exclude photochemical reactions. For Pu(IV) oxidation experiments, stock solutions were used to prepare 10^{-10} M ^{238}Pu(IV), 100 μM Fe(II), 0 to 20 mg/L HA, and 5 mM NaCl at the desired pH (3.5 or 6) and reach a total volume of 8 mL. These solutions were equilibrated for 0.5 h prior to addition of H_2O_2. Great care was taken to prepare Fe(II) solutions to prevent oxidation/precipitation. For the Fe(II) stock solution, an appropriate weight of $FeCl_2{\cdot}4H_2O$ was diluted in a few mL of hydrochloric acid (0.1 M) and then added to an appropriate volume of ultrapure water to give the desired pH and concentration of Fe(II). The Fe(II) stock

https://dx.doi.org/10.1021/acs.est.0c08195
Environ. Sci. Technol. 2021, 55, 1800−1810

Table 1. Reactions and Constants Used for Modeling Pu(VI/V) during Fe(II)−HA−Pu(IV) Oxidation by H_2O_2

no.	reactions	reaction rate constants pH 3.5	reaction rate constants pH 6
		Fenton Oxidation	
1	$Fe(II) + H_2O_2 \rightarrow Fe(III) + {}^{\bullet}OH + OH^-$	k_1 = 51 M^{-1} s^{-1}[171]	<keep-together>k_1' = 0.8 M^{-1} s^{-1}</keep-together>[d]
2	$Fe(III) + H_2O_2 \rightarrow Fe(II) + HO_2^{\bullet} + H^+$	$k_2 = 2 \times 10^{-3}$ M^{-1} s^{-1}[171]	[b]
3	$H_2O_2 + {}^{\bullet}OH \rightarrow HO_2^{\bullet} + H_2O$	$k_3 = 3.3 \times 10^7$ M^{-1} s^{-1}[171]	[b]
4	$Fe(III) + HO_2^{\bullet} \rightarrow Fe(II) + O_2 + H^+$	$k_4 = 7.8 \times 10^5$ M^{-1} s^{-1}[171]	[b]
5	$Fe(II) + {}^{\bullet}OH \rightarrow Fe(III) + OH^-$	$k_5 = 3.2 \times 10^8$ M^{-1} s^{-1}[171]	[b]
6	$Fe(II) + HO_2^{\bullet} \rightarrow Fe(III) + H2O2$	$k_6 = 1.3 \times 10^6$ M^{-1} s^{-1}[171]	[b]
7	$HO2\cdot + HO_2^{\bullet} \rightarrow H_2O_2 + O_2$	$k_7 = 2.3 \times 10^6$ M^{-1} s^{-1}[171]	[b]
8	$^{\bullet}OH + HO_2^{\bullet} \rightarrow H_2O + O_2$	$k_8 = 7.1 \times 10^9$ M^{-1} s^{-1}[171]	[b]
9	$^{\bullet}OH + {}^{\bullet}OH \rightarrow H_2O_2$	$k_9 = 5.2 \times 10^9$ M^{-1} s^{-1}[171]	[b]
10	$HO_2^{\bullet} \leftrightarrow O_2^{\bullet} + H^+$	k_{10f} = 1.14× 10^6; k_{10r} = 7.2× 10^{10}[70]	
11	$^{\bullet}OH + Pu(IV) \rightarrow Pu(VI/V)$	$k_{11} = 8 \times 10^7$ M^{-1} s^{-1}[d]	[b]
12	$Fe(II) + O_2 \rightarrow Fe(III) + HO_2^{\bullet}$		$k_{12} = 3.8 \times 10^{-6}$ M^{-1} s^{-1}[189]
		Effect of HA on Fenton Oxidation[a]	
13	$^{\bullet}OH + HA \rightarrow HA_{OX} + HO_2^{\bullet}$	k_{13} = 2.3 ×10^4 (mg C/L)$^{-1}$ s^{-1}[190]	[b]
14	$Fe(II) + HA \leftrightarrow Fe(II)-HA$	$K_{14} = 3.5 \times 10^5$ M−[170]	[b,c]
15	$Fe(III) + HA \rightarrow Fe(III)-HA$	$k_{15} = 1.2 \times 10^6$ M^{-1} s^{-1}[170]	[b]
16	$Fe(II)-HA + H_2O_2 \rightarrow Fe(III)-HA+ {}^{\bullet}OH$	k_{16} = 0.51 M^{-1} s^{-1}[d]	<keep-together>k_{16}' = 60 M− s^{-1}</keep-together>[d]
17	$Fe(II)-HA + {}^{\bullet}OH \rightarrow Fe(III)-HA+ OH^-$	$k_{17} = 10^{10}$ M^{-1} s^{-1}[170]	[b]
18	$Fe(II)-HA+ O_2 \rightarrow Fe(III)-HA + HO_2^{\bullet}$		$k_{18} = 6.1 \times 10^{-6}$ M^{-1} s^{-1}[170]
19	$^{\bullet}OH + Pu(IV)-HA \rightarrow Pu(VI/V)+ HA_{OX}$	$k_{19} = 6.3 \times 10^7$ M^{-1} s^{-1}[d]	[b]
		Pu(VI/V) Reduction by HA[a]	
20	$HA + Pu(VI/V) \rightarrow Pu(IV) + HA_{OX}$	k_{20} = 3 M^{-1} s^{-1}[d]	[b]

[a]Molecular weight of HA taken at 227 g/mol and 108 g C/mol based on the $C_9H_9NO_6$. [b]The rate constant at pH 6 is the same as that at pH 3.5. [c]Equilibrium reactions were written as separate forward and back reactions, with fast, non-rate-determining forward/back rate constants, and the pH was kept constant for each experiment. [d]Rate constants (in bold) fitted to data presented here.

solutions were prepared daily and kinetic experiments rapidly carried out to prevent the formation of polymeric Fe(III) species. In pH 3.5 experiments, the suspension pH was adjusted using NaOH/HCl. At pH 6, 0.5 mM MES was used as a buffer. MES did not appear to exhibit any influence on Pu redox behavior at our experimental timescales. pH was monitored and adjusted frequently with NaOH/HCl to maintain the pH at 6.0 ± 0.3. Samples were withdrawn at predetermined time intervals for Pu fractionation and oxidation state analysis. Pu(IV) reduction by Fe(II) is very slow. Felmy et al. (2011) found that Pu(IV) reduction by 1 mM Fe(II) was not observed even in the presence of goethite for as long as 16 days.[55]

Three sets of control experiments were conducted. In the first set of control experiments, H_2O_2 was excluded from the batch experiments in order to confirm that the initial Pu was in the Pu(IV) oxidation state and in a colloidal form associated with HA. In the second set of control experiments, designed to test the role of $^{\bullet}OH$, *tert*-butanol (>99.5%, to achieve 10 mM in solution) was added prior to H_2O_2 addition to rapidly quench any $^{\bullet}OH$ generated after H_2O_2 addition. In the third set of control experiments, Pu(VI) was used in batch experiments to quantify Pu(VI) reduction rates in the presence of HA at pH 3.5 and pH 6. Reactions were initiated by adding HA ranging from 0−20 mg/L to a solution containing 10^{-10} M $^{238}Pu(VI)$ at pH 3.5 or pH 6 and aliquots were periodically collected to determine the concentrations of Pu(V/VI) over time.

A separate set of experiments was performed to characterize the kinetics of colloid formation and colloid charge characteristics. The particle size distribution and zeta potential of Pu−HA−Fe colloidal suspensions upon addition of H_2O_2 was evaluated by dynamic light scattering (DLS) (Zetasizer Nano, Malvern Instruments, UK) to generate time-resolved changes. In these experiments, Pu was omitted from the DLS experiments to limit radiologic hazards associated with these large sample volume experiments; the presence of Pu would not significantly impact particle size and zeta potential of the system given its extremely low concentration (10^{-10} M) relative to Fe and HA in solution. The HA−Fe(II) suspensions were prepared in the same way as the Pu(IV)−HA−Fe(II) oxidation experiments but without addition of Pu and using large sample volumes (1 L). The suspension was mixed with magnetic stirring of 400 rpm to simulate the rotation condition in Pu batch experiments. The first points were measured before addition of H_2O_2. For each DLS and zeta potential measurement, approximately 1 mL of the suspension was added into a polystyrene cuvette and analyzed immediately.

2.3. Analytical Methods. The concentration of Pu was quantified by liquid scintillation counting (LSC; Tri-Carb 2900 TR liquid scintillation analyzer, PerkinElmer). The oxidation state of Pu(IV) and Pu(VI) stock solutions was confirmed by LSC in combination with solvent extraction method, which uses 0.5 M bis(ethylhexyl) phosphoric acid (HDEHP) in hexane and 0.025 M 4-benzoyl-3-methyl-1-phenyl-2-pyrazolin-5-one (PMBP) in hexane as the extractants.[56] The oxidation state of the Pu(IV) and Pu(VI) stock solutions was verified as >90% Pu(IV) and >95% Pu(VI), respectively. The HA concentration in the stock solution was measured by TOC (Shimadzu TOC-L TOC analyzer). The H_2O_2 solution (30% w/w) was standardized by titration with $KMnO_4$ and stored at 4 °C.[57]

At each sampling event and in each experiment, analysis of Pu oxidation state was performed using the lanthanum fluoride

https://dx.doi.org/10.1021/acs.est.0c08195
Environ. Sci. Technol. 2021, 55, 1800−1810

coprecipitation method where LaF_3 coprecipitates with Pu(III) and Pu(IV) and leaves Pu(V) and Pu(VI) in the aqueous phase.[58] The amount of Pu(III/IV) and Pu(V/VI) can be determined by the difference when measuring the concentration of plutonium in solution before and after addition of LaF_3. Note that this procedure cannot distinguish between Pu(V) and Pu(VI), so the data are reported as combined Pu(V/VI). This procedure also cannot distinguish between Pu(III) and Pu(IV). However, as we explain later in the text, the likelihood of forming Pu(III) under these conditions and at these timescales was considered unlikely. As a result, we report the reduced Pu oxidation state simply as Pu(IV).

At each sampling event and in each experiment, Pu was characterized as truly dissolved (<3000 Da, corresponding to ~1−3 nm), colloidal (1−3 nm to 200 nm), and particulate (>200 nm). These fractions were operationally separated by 3000 Da ultrafiltration membranes (EMD, Millipore) and centrifugation at 13,000*g* for 10 min (size cutoff ~200 nm). The concentration of Pu in each size fractions was then quantified by LSC.

H_2O_2 in the stock solution and samples was measured by spectrophotometric method on the basis of the oxidative coloration of DPD in the horseradish peroxide (POD)-catalyzed reaction.[57]

2.4. Kinetic Modeling of Pu(IV) Oxidation. A model of Pu redox kinetics was developed by considering Fenton oxidation of Pu(IV) and Pu(V/VI) reduction by HA. Most other Fenton reaction rate constants have been previously reported in the literature and were used here without adjustment (Table 1). Only a small number of Pu redox reaction rates and Fenton reaction rates at neutral pH were derived from our experiments and used to capture the observed Pu redox transformations. The development of our model was based on the following conceptual framework. First, the overall Pu(V/VI) → Pu(IV) reduction rate in the presence of HA was quantified using Pu(VI) reduction experiments (Figure S2). Pu(VI) → Pu(IV) reduction does not occur in a single step. Pu(VI) is first reduced to Pu(V) and then to Pu(IV). However, recent evidence suggests that Pu(VI) → Pu(V) is fast and Pu(V) → Pu(IV) is the rate-limiting step.[31] As a result, we assume here that the reduction rate of Pu(VI) → Pu(IV) can be directly applied to Pu(VI/V) → Pu(IV). Second, we assumed that $^{\bullet}OH$ was the only reactive intermediate generated from H_2O_2 decomposition by Fe(II) and Fe(II)−HA that oxidized Pu(IV). This assumption was made to limit the number of fitting reaction constants in our model. Third, formation of Fe(II)−HA complexes was assumed to impact H_2O_2 decomposition Fenton reaction rates, as has been reported in the literature. Fourth, formation of Pu(IV)−HA complexes limits Pu(IV) oxidation by $^{\bullet}OH$. Fifth, we assumed that the rate of aqueous Pu(IV) oxidation by hydroxyl radicals was the same at pH 3.5 and pH 6. While the speciation of Pu(IV) is known to vary as a function of pH and may affect oxidation rates, $Pu(OH)_3^+$ was the dominant species at these two pH conditions (Figure S1). All reactions and their rate constants are summarized in Table 1, and the rate equations were modeled using MATLAB 2019a. Importantly, the modeling effort was intended to support the experimental observation of transient Pu redox transformations and their potential impact on the fate of Pu in natural systems rather than to develop a mechanistic predictive capability. The fitted Pu reaction constants should be considered empirical in nature as they do not directly address impacts of all Fenton radicals in solution nor the impact of Fe(III) oxide formation and potential surface-mediated redox processes. Nevertheless, our modeling effort indicates that Fenton reaction rates reported in the literature can be integrated with Pu oxidation and reduction rates to effectively capture the transient Pu redox transformations under our experimental conditions. This, in effect, is the first step in quantifying Pu redox processes that may control aqueous Pu migration across complex redox gradients.

3. RESULTS AND DISCUSSION

3.1. Effect of HA on Pu(IV) Oxidation. At pH 3.5, addition of H_2O_2 to systems containing Pu(IV)−HA−Fe(II) resulted in Pu(IV) oxidation, where the rate and extent of oxidation were dependent on HA concentration ranging from 0 to 20 mg/L HA (Figure 1a). When HA was absent, as shown in solid red diamonds, Pu(IV) was rapidly oxidized within the first 0.5 h of H_2O_2 addition, and then the oxidation got much slower after the initial stage. With HA present, Pu(IV) oxidation was significantly inhibited, even with as little as 0.5 mg/L HA. Increasing HA concentration led to greater oxidation inhibition. For example, 86%, 33%, and 12% of the Pu(IV) were oxidized after 26 h with zero, 0.5 mg/L, and 5 mg/L HA, respectively. The apparent inhibitory effect of HA on Pu(IV) oxidation could be explained by three mechanisms. First, the oxidized Pu(V/VI) are quickly reduced back to Pu(IV) in the presence of HA (Figure S2), consistent with the previous observation where higher oxidation states (Pu(V/VI)) can be reduced rapidly to Pu(IV) and even further to Pu(III) by HA.[6,59,60] Second, HA-Fe(II) complex formation may lead to inefficient H_2O_2 decomposition and low $^{\bullet}OH$ production. Work by Bissey et al.[61] found that soil organic matter will not affect H_2O_2 decomposition rates or $^{\bullet}OH$ activity at pH 3. However, their experimental conditions were quite different and results may not be transferrable to our experimental conditions. Third, Pu(IV)−HA complexes may be resistant to oxidation by $^{\bullet}OH$. Additional mechanisms such as direct reactions between HA and H_2O_2 are less likely to play a role, considering the low reported rates (7.97×10^{-12} s^{-1}).[62] In the following section, our modeling efforts attempt to quantify the impact of each of these mechanisms. However, given the limited scope of our experimental effort and the complexity of the Fenton reaction chemistry, further examination of specific mechanisms controlling Fenton reaction Pu(IV) oxidation is warranted.

At pH 6, the extent of Pu(IV) oxidation was lower than at pH 3.5 in the absence of HA (Figure 1b). This is likely due to the lower oxidant production of Fenton reactions at higher pH. The fraction of Pu(V/VI) was 45% at 26 h at pH 6, which is much lower than that of 86% at pH 3.5 (Figure 1a). Interestingly, when the HA concentration is higher than 5 mg/L, Pu(IV) was rapidly oxidized within the first 1−2 h to Pu(V/VI) but gradually reduced back to Pu(IV) over the next 30 h (Figure 1b). Initial accelerated Pu(IV) oxidation is likely due to the ability of HA to enhance the oxidation efficiency of the Fenton reaction at neutral pH.[63−66] HA−Fe(II) complexes are known to react more rapidly with H_2O_2 than Fe(II)−aquo complexes, thereby increasing the rate of hydroxyl radical formation significantly at neutral pH but negligibly at pH 3.5.[65,67,68] Bissey et al. has reported that NOM increased the rate of hydroxyl radical generation at neutral pH, while it did not affect H_2O_2 decomposition rates or the activity of hydroxyl radical at pH 3.5.[61] Importantly, the rate of Pu(V/VI)

https://dx.doi.org/10.1021/acs.est.0c08195
Environ. Sci. Technol. 2021, 55, 1800−1810

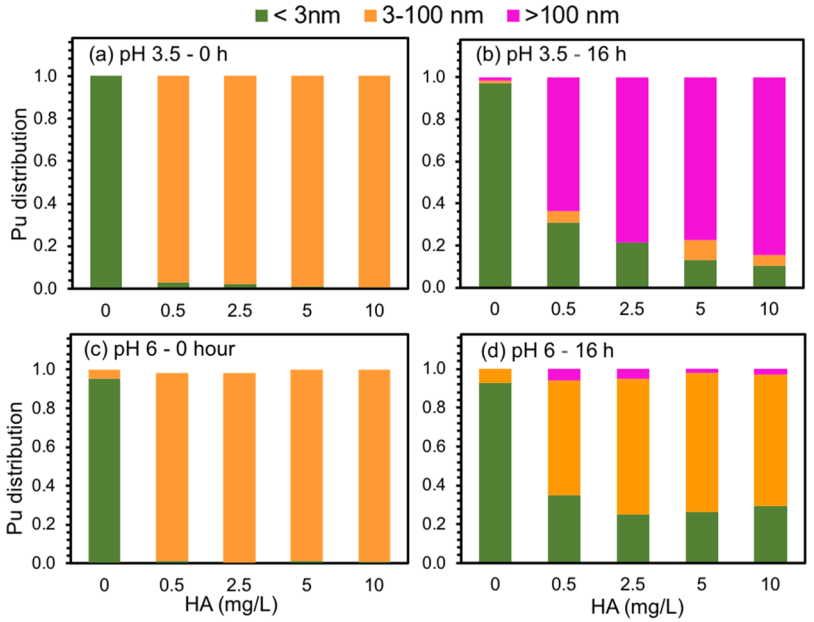


Figure 2. Percentage of Pu present in different size fractions is shown (a) at pH 3.5 before H_2O_2 added, (b) at pH 3.5, 16 h after the addition of H_2O_2, (c) at pH 6 before H_2O_2 is added, and (d) at pH 6, 16 h after the addition of H_2O_2. Experimental conditions were the same as in Figure 1. $Fe(II)_0$ = 100 μM, $Pu(IV)_0$ = 10^{-10} M, H_2O_2 = 100 μM, NaCl = 5 mM.

reduction positively correlates with HA concentration (Figure 1b), consistent with our control experiments showing HA-facilitated reduction of Pu(VI) (Figure S2).

3.2. Kinetic Modeling. To identify and quantify the observed Pu redox reactions, we developed a model of Pu redox reaction kinetics based on published studies of Fenton–HA reaction kinetics combined with Fenton oxidation of Pu(IV) and Pu(V/VI) reduction by HA fit to our experimental data (Table 1). The rate constant for Pu(IV) oxidation by $^{\bullet}OH$ (k_{11}) was determined using the Pu(IV)–Fe(II)–H_2O_2 (in the absence of HA) data at pH 3.5 (Figure 1a). Under this condition, Pu(IV) was rapidly oxidized within the initial 0.5 h followed by much slower oxidation, consistent with oxidation efficiency trend from the Fe(II)-catalyzed H_2O_2 process. Although Pu(IV) may be present as different hydrated species, the k_{11} derived from the pH 3.5 data was assumed to be independent of pH for practical purposes and was applied to our model at pH 6.

No previous rate constants were available for Fe(II) reaction with H_2O_2 at pH 6 ($k1'$) (Table 1). Although Miller et al. reported values for H_2O_2-mediated oxidation of Fe(II) at pH 7,[69,70] a very high rate constant was reported with an emphasis on photo-Fenton reaction and without considering the generation of oxidizing intermediates in the reaction. To limit the number of fitting parameters in our model, the pH effect on Fenton reactions was addressed by only adjusting k_1' (Table 1). Thus, k_1' = 0.8 M^{-1} s^{-1} was a fitted value, while other Fenton reaction rate constants (k_2 to k_{11}) were held constant and their values taken from pH 3.5 data available in the literature.[71]

At pH 3.5 and with the addition of HA, the slow oxidation of Fe(II)–HA complexes by H_2O_2 (k_{16}), formation of Pu(IV)–HA complexes resistant to oxidation by $^{\bullet}OH$ (k_{19}), and Pu(V/VI) reduction by HA (k_{20}) all contributed to overall lower Pu(V/VI) concentrations in the system. We found that the rate of Pu(V/VI) reduction by HA and rate of Fe(II)–HA reaction with H_2O_2 play important roles in controlling Pu(V/VI) concentration in the system. Note that the rate constant of Pu(V/VI) reduction by HA was determined from Pu(VI) reduction control experiments (Figure S3). The rate of Pu(VI) reduction by HA (k_{20}) was independent of pH (Figure S2).

At pH 6, Fe(II)–HA complexes reacted with H_2O_2 faster than at pH 3.5. Fe(II)–HA complexes also reacted faster than the Fe(II)–aquo complexes, resulting in a higher overall rate of $^{\bullet}OH$ production ($k16'$).[70,72,73] An increase in the rate of $^{\bullet}OH$ formation with increasing concentration of HA has been reported for a stoichiometric Fenton system at pH $\geq$ 4.5.[67,72,74] This increased rate of $^{\bullet}OH$ formation leads to very rapid oxidation of Pu(IV). However, after H_2O_2 is largely consumed (Figure S3), Pu(V/VI) is found to reduce back to Pu(III/IV) by HA (Figure 1b).

The predicted rapid oxidation of Fe(II) is shown in Figure S4, implying the rapid formation of Fe(III) oxide precipitates or HA–Fe(III) oxide heteroaggregates upon H_2O_2 addition. However, the presence of Fe(III) oxide precipitates or heteroaggregates is not likely to dominate Pu redox transformations at the reaction timescales examined here (~30 h).[49,75] Instead, our modeling suggests that transient Pu redox cycling is controlled by Pu(IV) oxidation by reactive intermediates generated from Fe(II) or Fe(II)–HA reaction with H_2O_2 and Pu(V/VI) reduction by HA, which are dependent on pH and HA concentration. While H_2O_2 decomposition was accelerated by HA at both pH 3.5 and 6 (Figure S3), the impact of HA on Pu(IV) oxidation rates had opposite effects: lowering oxidations rates at pH 3.5 and increasing oxidation rates at pH 6.

Overall, our kinetic model accounts for the observed trends in Pu redox transformations. Importantly, only 6 reaction rate constants were used to independently fit the data at both pHs. The remaining 18 rate constants were taken directly from the literature without adjustment. The ability of our model to predict general trends in Pu behavior and H_2O_2 consumption is promising. However, a number of simplifying assumptions were made during model development. As a result, additional

https://dx.doi.org/10.1021/acs.est.0c08195
Environ. Sci. Technol. 2021, 55, 1800–1810

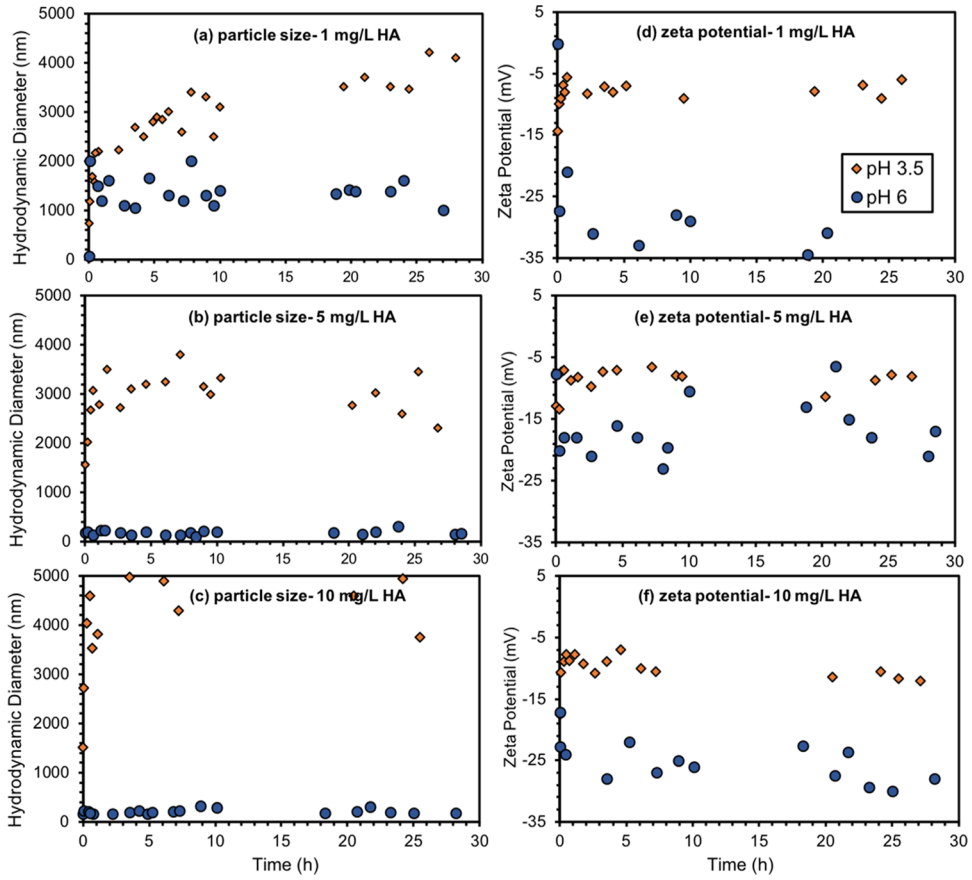


Figure 3. Evolution of the in situ measured hydrodynamic diameters and zeta potential of the HA−Fe(II) particles with H_2O_2 at HA concentrations of 0, 5, or 10 mg/L at pH 3.5 (yellow diamonds) and pH 6 (blue dots).

data are certainly needed to develop a more robust predictive model.

3.3. Role of •OH in Pu(IV) Oxidation. A set of control experiments were performed to test the role of •OH in Pu(IV) oxidation. The presence of •OH was quenched by adding *tert*-butanol to a set of batch experiments prior to H_2O_2 addition. *tert*-Butanol is an effective radical scavenger as indicated by the high reaction rate constant when it reacts with •OH ($k = 9.7 \times 10^8$ M^{-1} s^{-1}).[76,77] In solutions with 10 mg/L HA at pH 6, the oxidation of Pu(IV) is completely inhibited by the presence of 10 mM *tert*-butanol (Figure S5b), revealing •OH as the dominant Pu(IV) oxidant under this condition. It is more difficult to assess the role of •OH in solutions with 10 mg/L HA at pH 3.5 because Pu(IV) oxidation was already low even without *tert*-butanol (Figure S5a). In the absence of HA, addition of *tert*-butanol significantly lowered the Pu(IV) oxidation at both pH 3.5 and 6. Pu(VI/V) concentrations at 26 h were ∼50% lower at both pHs when compared to *tert*-butanol-free experiments, indicating that •OH was an important reactive species for Pu(IV) oxidation. However, the incomplete quenching of Pu(IV) oxidation suggests the existence of other reactive intermediates. At pH 3.5, *tert*-butanol was reported to react mainly with •OH. The existence of other radicals such as $HO_2^•$ may also contribute to oxidation for Pu(IV) in our system. At near neutral pH, a number of studies have suggested formation of oxidizing species other than •OH radicals, for example, Fe(IV), by way of the Fenton reaction.[78−80] These additional oxidizers may also play a role in Pu(IV) oxidation at pH 6. Nevertheless, at both pH 3.5 and 6, •OH appears to play an important if not dominant role in Pu(IV) oxidation. Furthermore, Pu(IV) oxidation by O_2 is also thermodynamically favorable at such pH. However, oxidation rates are sufficiently slow to not affect our experiments.

3.4. Pu Mobility. In addition to redox transformations, the presence of HA and Fe species can also greatly influence the fate and transport of Pu by affecting the Pu-associated particle size distribution. In the absence of HA, all Pu was present in the aqueous phase before and after H_2O_2 oxidation (Figure 2). Prior to H_2O_2 addition, Pu(IV) was present in the aqueous phase because no solid phase was present in solution. After H_2O_2 addition, formation of Fe(III) oxides was initiated. However, Pu(IV) was simultaneously oxidized to Pu(V/VI). The predominance of Pu(V/VI) in solution (weak sorbers as both pH 3.5 and 6) and the small amount of Fe(III) oxide formed (∼0.01 g/L maximum based on 100 μM Fe) explains why Pu remains in the aqueous phase even after H_2O_2 addition and Fe(III) oxide precipitation. In the presence of HA (and prior to H_2O_2 addition), ultrafiltration and centrifugation data show that Pu(IV) was primarily bound to HA as Pu−HA colloidal complexes even at HA concentration as low as 0.5 mg/L (Figure 2a, c). The formation of monomeric Pu(IV)−HA complexes at concentrations up to 10^{-8} M Pu(IV) has been observed in batch studies[81] as well as a spectroscopy study using Pu L3-edge XAFS.[82] Based on Pu solubility data reported by Neck et al.,[11] the formation of PuO_2 intrinsic colloids was not likely to occur under trace Pu conditions used here.

https://dx.doi.org/10.1021/acs.est.0c08195
Environ. Sci. Technol. 2021, 55, 1800−1810

A former study of HA−Fe(II) complexation by Liao et al. found that at neutral pH, Fe(II) was composed primarily of HA−Fe(II) colloidal complexes when the molar ratio of C/Fe is higher than 0.5.[42] Based on HA molecular weight calculations in our experiments, most of the Fe(II) is present as Fe(II)−HA colloidal complexes in the 10 to 20 mg/L HA samples (prior to H_2O_2 addition). However, some free Fe(II) will be present in samples with HA concentrations below 10 mg/L. At pH 3.5, Fe(II) complexation with HA is much weaker and a larger fraction of Fe(II) is likely to be aqueous.[83]

Pu analysis of samples after reaction with H_2O_2 revealed that truly dissolved Pu accounts for only a small fraction of total Pu. At pH 3.5, the majority (>80%) of Pu exists as large heteroaggregates (>200 nm) (Figure 2b), whose concentration increased with increasing HA concentration. Truly dissolved Pu (<1−3 nm) correspondingly dropped from 20 to 5%, which was consistent with Pu(V/VI) concentrations in solution (Figure 1). The aggregation is likely caused by the generation of Fe(III) oxide which neutralizes the negative surface charge of humic acid, driving heteroaggregation through electrostatic and van der Waals attractions.[42]

In contrast to pH 3.5 data, Pu(IV) was found primarily in a colloidal form at pH 6 across the range of HA concentrations examined here (Figure 2d). Such differences in Pu size at the two pHs can be attributed to pH-dependent negative charge of HA. Previous study by Sparks et al. showed a gradual increase in HA negative charge with increasing pH due to the dissociation of protons from carboxylic and phenolic functional groups.[84] Given that the surface charge properties of Pu−HA−Fe(III) oxide particles govern aggregation behavior, charge neutralization at pH 3.5 likely leads to particle aggregation. At pH 6, the negative surface charge of Pu−HA−Fe(III) oxide particles will be higher, resulting in less aggregation. Clearly, pH plays a dominant role in the formation of Pu−HA−Fe(III) oxide colloids and heteroaggregates and will affect colloid-facilitated transport of these Pu-containing particulates.

3.5. Colloid Aggregation Kinetics. The partitioning of Pu between the aqueous, colloidal, and HA−Fe(III) oxide heteroaggregate fractions in these experiments was largely controlled by the aggregation behavior of colloidal particles in the system. We used time-resolved DLS measurements to determine the average hydrodynamic diameter of particles in our experiments as a function of time. With HA ranging from 1 to 10 mg/L, the average hydrodynamic particle size upon addition of H_2O_2 exhibits a distinct pH-dependence (Figure 3). At pH 3.5, the hydrodynamic diameter increased rapidly, indicating the formation of large HA−Fe(III) oxide hetero-aggregates. This aggregation behavior was consistent with the fast generation of Fe(III) in the Fenton reaction, where Fe(III) destabilized humic acid and induced the formation HA−Fe(III) oxide heteroaggregates. The zeta potential of particles was measured concurrently and also increased from around −15 to −5 mV. This is likely due to charge neutralization which leads to colloid aggregation. At pH 6, the particle size was overall much smaller, and no formation of large heteroaggregates was observed, particularly when HA was >5 mg/L. The HA−Fe(III) oxide colloids had a more negative zeta potential at pH 6 which minimized colloid aggregation. Similar patterns observed for Pu partitioning among the three size fractions (Figure 2) and HA−Fe particle size distribution (Figure 3) are strong indicators of the close association of Pu with HA−Fe(III) colloids and heteroaggregates. Importantly, the results indicate that surface charge characteristics of HA−Fe(III)−Pu nanoparticles may facilitate colloid transport at neutral pH, consistent with observations of significant Pu transport in association with Fe(III) oxide nanoparticles at the Mayak site, Russia.[23]

3.6. Pu Speciation in the Presence of HA. Indirect information about the oxidation state of aqueous and particulate Pu in the presence of HA can be gained from comparing total Pu(V/VI) concentrations in our experiments to measured aqueous (<1−3 nm) Pu concentrations. At pH 3.5, aqueous Pu (<1−3 nm) concentrations as a function of reaction time and HA concentration (Figure S6) correlate strongly with measured Pu(V/VI) concentrations (Figure 1a). To test this relationship, all samples for which Pu(V/VI) concentration and aqueous (<1−3 nm) Pu concentration data were available in the presence of HA were plotted on a single figure (Figure 4). The specific experimental conditions of each

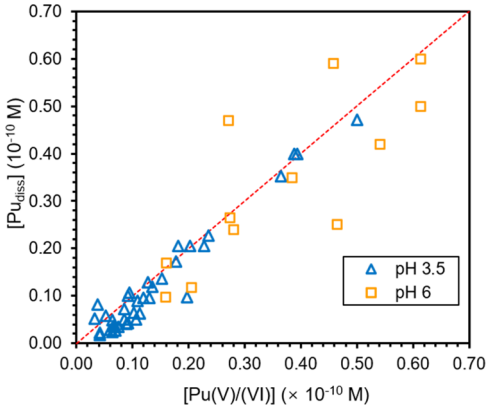


Figure 4. Correlation plot of Pu(V/VI) concentration (based on LaF_3 coprecipitation) in batch samples reported herein and aqueous Pu concentration (<1−3 nm, based on ultrafiltration) at each sampling event of pH 3.5 and pH 6.

sampling event are presented in Table S1, which comprises a summary of all batch experiments. The linear correlation between concentration of Pu(V/VI) (measured using the LaF_3 precipitation method) and Pu in aqueous phase (<1−3 nm, based on ultrafiltration) at pH 3.5 indicates that Pu(V/VI) mainly exists as aqueous Pu not associated with HA or colloidal particles, while Pu(IV) is complexed with HA and Fe(III), which form colloids and heteroaggregates. Similar observations of more mobile Pu(V) and Pu(VI) compared to Pu(IV) have been previously reported.[10,29,85] Cusnir et al. indicates that Pu(V) is more mobile than Pu(IV) when comparing the rates of Pu(IV)−NOM and Pu(V)−NOM dissociations via diffusive gradients in thin-film techniques.[29] Furthermore, Chen et al. studied the effects of NOM on Pu sorption behavior and indicated that Pu(IV) is bonded more strongly to NOM, while Pu(V/VI) sorbs more readily to the prevailing solid surfaces.[41] The pH 6 data produce significantly more scatter (Figure 4), suggesting that the correlation is not as robust. Nevertheless, it remains apparent that Pu(V/VI) is the predominant oxidation state in the aqueous (<1−3 nm) phase.

To further support our notion of weak Pu(V/VI) interaction with HA, we simulated Np(V)−HA complexation (Figure S7) at our experimental conditions. Np(V) and Pu(V) sorption and complexation are expected to be broadly similar, while Np(V) is less susceptible to redox transformations common to Pu(V).[86,87] The complexation constants of Np(V) with humic

https://dx.doi.org/10.1021/acs.est.0c08195
Environ. Sci. Technol. 2021, 55, 1800−1810

acid were available from the literature and derived from anion exchange chromatography combined with radiometric detection.[87,88] Based on these equilibrium complexation constants, at pH 3.5 the formation of Np(V)−HA complexes is negligible compared with total Np(V) even when HA is as high as 20 mg/L (Figure S7). At pH 6, Np(V)−HA complexes account for a significant fraction of total Np(V) at high HA concentrations. For example, $[Np(V)-HA]/[Np(V)_{total}]$ fraction was calculated to be 36% and 73% at 10 and 20 mg/L HA, respectively. The fact that we did not observe such high complexed fractions with Pu(VI/V) (Figure 4) is probably because Pu(V) was rapidly reduced to Pu(IV) once associated with HA.

4. ENVIRONMENTAL IMPLICATIONS

Based on our study, it is apparent that transient Pu redox reactions that occur during the mixing of surface water and groundwater or the infiltration of surface water into sediments can play an important role in the transient mobilization of Pu as Pu(V/VI), particularly at neutral pH. The presence of NOM would typically be thought to reduce any oxidized forms of Pu and, thus, lessen aqueous Pu migration or increase the potential for colloid-facilitated transport. However, our experimental results indicate that Pu(IV)−HA−Fe(II) colloids are subject to transient oxidation in the presence of H_2O_2, especially at near neutral pH. Indeed, HA can significantly accelerate Pu oxidation to Pu(V/VI). Our results suggest that the observations and conceptual models of enhanced Pu migration reported in the studies by Molz et al. and Maloubier et al. may indeed be explained by the transient Pu oxidation that occurs during the infiltration of H_2O_2-containing water into sediments.[22,52] However, high concentrations of NOM may also decrease Pu migration by facilitating the reduction of Pu(V/VI), as observed by Maloubier et al.[15] Indeed, the subsurface is a highly complex and heterogeneous environment that can exhibit dynamic geochemical conditions compared to systems presented in this study. Ongoing research will extend the framework developed here by evaluating the role of numerous variables (e.g., extended pH range, H_2O_2 concentrations, and NOM compositions). Identification of processes and mechanisms that control metal cycling and quantification of their reaction rates remains a significant challenge in environmental science.

■ ASSOCIATED CONTENT

Supporting Information

The Supporting Information is available free of charge at https://pubs.acs.org/doi/10.1021/acs.est.0c08195.

Pu(IV) speciation distribution dependent on pH, Pu(VI) reduction by HA, H_2O_2 decomposition during Pu oxidation, impact of *tert*-butanol on Pu(IV) oxidation, Np(V) complexation with HA, and experimental conditions of the points in Figure S4 (PDF)

■ AUTHOR INFORMATION

Corresponding Author

Chao Pan − *Glenn T. Seaborg Institute, Physical and Life Sciences Directorate, Lawrence Livermore National Laboratory, Livermore, California 94550, United States;* orcid.org/0000-0001-7309-0711; Email: chaopan6649@gmail.com

Authors

Yongqin Jiao − *Biosciences and Biotechnology Division, Physical and Life Sciences Directorate, Lawrence Livermore National Laboratory, Livermore, California 94550, United States;* orcid.org/0000-0002-6798-5823

Annie B. Kersting − *Glenn T. Seaborg Institute, Physical and Life Sciences Directorate, Lawrence Livermore National Laboratory, Livermore, California 94550, United States*

Mavrik Zavarin − *Glenn T. Seaborg Institute, Physical and Life Sciences Directorate, Lawrence Livermore National Laboratory, Livermore, California 94550, United States;* orcid.org/0000-0002-2426-6706

Complete contact information is available at: https://pubs.acs.org/10.1021/acs.est.0c08195

Notes

The authors declare no competing financial interest.

■ ACKNOWLEDGMENTS

This work was performed with funding from the Department of Energy, Office of Science, Biological and Environmental Research, Subsurface Biogeochemical Research program (SCW1053). Work was performed under the auspices of the U.S. Department of Energy by Lawrence Livermore National Laboratory under Contract DE-AC52-07NA27344 (LLNL-JRNL-808740).

■ REFERENCES

(1) Ikeda-Ohno, A.; Shahin, L. M.; Howard, D. L.; Collins, R. N.; Payne, T. E.; Johansen, M. P. Fate of plutonium at a former nuclear testing site in Australia. *Environ. Sci. Technol.* **2016**, *50*, 9098−9104.

(2) Montero, P. R.; Sánchez, A. M. Plutonium contamination from accidental release or simply fallout: study of soils at Palomares (Spain). *J. Environ. Radioact.* **2001**, *55*, 157−165.

(3) Smith, D. K.; Finnegan, D. L.; Bowen, S. M. An inventory of long-lived radionuclides residual from underground nuclear testing at the Nevada test site, 1951−1992. *J. Environ. Radioact.* **2003**, *67*, 35−51.

(4) Morris, K.; Butterworth, J. C.; Livens, F. R. Evidence for the remobilization of Sellafield waste radionuclides in an intertidal salt marsh, West Cumbria, UK. *Estuarine, Coastal Shelf Sci.* **2000**, *51*, 613−625.

(5) Hu, Q.-H.; Weng, J.-Q.; Wang, J.-S. Sources of anthropogenic radionuclides in the environment: a review. *J. Environ. Radioact.* **2010**, *101*, 426−437.

(6) Choppin, G. R. Redox speciation of plutonium in natural waters. *J. Radioanal. Nucl. Chem.* **1991**, *147*, 109−116.

(7) Morgenstern, A.; Choppin, G. Kinetics of the reduction of $Pu(V)O_2^+$ by hydrogen peroxide. *Radiochim. Acta* **1999**, *86*, 109−114.

(8) Begg, J. D.; Zavarin, M.; Zhao, P.; Tumey, S. J.; Powell, B.; Kersting, A. B. Pu(V) and Pu(IV) sorption to montmorillonite. *Environ. Sci. Technol.* **2013**, *47*, 5146−5153.

(9) Powell, B. A.; Fjeld, R. A.; Kaplan, D. I.; Coates, J. T.; Serkiz, S. M. $Pu(V)O_2^+$ adsorption and reduction by synthetic magnetite (Fe_3O_4). *Environ. Sci. Technol.* **2004**, *38*, 6016−6024.

(10) Joseph, C.; Balboni, E.; Baumer, T.; Treinen, K.; Kersting, A. B.; Zavarin, M. Plutonium desorption from nuclear melt glass-derived colloids and implications for migration at the Nevada National Security Site, USA. *Environ. Sci. Technol.* **2019**, *53*, 12238−12246.

(11) Neck, V.; Altmaier, M.; Seibert, A.; Yun, J.-I.; Marquardt, C. M.; Fanghänel, T. Solubility and redox reactions of Pu(IV) hydrous oxide: Evidence for the formation of PuO_{2+x} (s, hyd). *Radiochim. Acta* **2007**, *95*, 193−207.

(12) Conroy, N. A.; Zavarin, M.; Kersting, A. B.; Powell, B. A. Effect of natural organic matter on plutonium sorption to goethite. *Environ. Sci. Technol.* **2016**, *51*, 699−708.

(13) Zimmerman, T.; Zavarin, M.; Powell, B. A. Influence of humic acid on plutonium sorption to gibbsite: Determination of Pu-humic acid complexation constants and ternary sorption studies. *Radiochim. Acta* **2014**, *102*, 629−643.
(14) Boggs, M. A.; Jiao, Y.; Dai, Z.; Zavarin, M.; Kersting, A. B. Interactions of Plutonium with Pseudomonas sp. Strain EPS-1W and Its Extracellular Polymeric Substances. *Appl. Environ. Microbiol.* **2016**, *82*, 7093−7101.
(15) Vázquez-Campos, X.; Kinsela, A. S.; Bligh, M. W.; Harrison, J. J.; Payne, T. E.; Waite, T. D. Response of microbial community function to fluctuating geochemical conditions within a legacy radioactive waste trench environment. *Appl. Environ. Microbiol.* **2017**, *83*, No. e00729.
(16) Santschi, P. H.; Xu, C.; Zhang, S.; Schwehr, K. A.; Grandbois, R.; Kaplan, D. I.; Yeager, C. M. Iodine and plutonium association with natural organic matter: A review of recent advances. *Appl. Geochem.* **2017**, *85*, 121−127.
(17) Geckeis, H.; Salbu, B.; Schafer, T.; Zavarin, M. *Environmental Chemistry of Plutonium*; Lawrence Livermore National Lab. (LLNL): Livermore, CA (United States), 2019.
(18) Choppin, G. R. Actinide speciation in the environment. *J. Radioanal. Nucl. Chem.* **2007**, *273*, 695−703.
(19) Kaplan, D. I.; Powell, B. A.; Demirkanli, D. I.; Fjeld, R. A.; Molz, F. J.; Serkiz, S. M.; Coates, J. T. Influence of oxidation states on plutonium mobility during long-term transport through an unsaturated subsurface environment. *Environ. Sci. Technol.* **2004**, *38*, 5053−5058.
(20) Powell, B. A.; Duff, M. C.; Kaplan, D. I.; Fjeld, R. A.; Newville, M.; Hunter, D. B.; Bertsch, P. M.; Coates, J. T.; Eng, P.; Rivers, M. L. Plutonium oxidation and subsequent reduction by Mn(IV) minerals in Yucca Mountain tuff. *Environ. Sci. Technol.* **2006**, *40*, 3508−3514.
(21) Serkiz, A. I.; Zhou, D.; Boukhalfa, H.; Tarimala, S.; Ware, S. D.; Keller, A. A. Dispersion stability and electrokinetic properties of intrinsic plutonium colloids: implications for subsurface transport. *Environ. Sci. Technol.* **2013**, *47*, 5626−5634.
(22) Maloubier, M.; Emerson, H.; Peruski, K.; Kersting, A. B.; Zavarin, M.; Almond, P. M.; Kaplan, D. I.; Powell, B. A. Impact of natural organic matter on plutonium vadose zone migration from an $NH_4Pu(V)O_2CO_3(s)$ source. *Environ. Sci. Technol.* **2020**, *54*, 2688−2697.
(23) Novikov, A. P.; Kalmykov, S. N.; Utsunomiya, S.; Ewing, R. C.; Horreard, F.; Merkulov, A.; Clark, S. B.; Tkachev, V. V.; Myasoedov, B. F. Colloid transport of plutonium in the far-field of the Mayak Production Association, Russia. *Science* **2006**, *314*, 638−641.
(24) Malcolm, R. L. The uniqueness of humic substances in each of soil, stream and marine environments. *Anal. Chim. Acta* **1990**, *232*, 19−30.
(25) Aiken, G. R.; McKnight, D.M.; Wershaw, R.L.; MacCarthy, P. *Humic Substances in Soil, Sediment, and Water. Soil Science* 1986, *142* (5), 323.
(26) Pan, C.; Troyer, L. D.; Liao, P.; Catalano, J. G.; Li, W.; Giammar, D. E. Effect of humic acid on the removal of chromium(VI) and the production of solids in iron electrocoagulation. *Environ. Sci. Technol.* **2017**, *51*, 6308−6318.
(27) Liao, P.; Pan, C.; Ding, W.; Li, W.; Yuan, S.; Fortner, J. D.; Giammar, D. E. Formation and transport of Cr(III)-NOM-Fe colloids upon reaction of Cr(VI) with NOM-Fe(II) colloids at anoxic-oxic interfaces. *Environ. Sci. Technol.* **2020**, *54*, 4256−4266.
(28) Kleber, M.; Lehmann, J. Humic substances extracted by alkali are invalid proxies for the dynamics and functions of organic matter in terrestrial and aquatic ecosystems. *J. Environ. Qual.* **2019**, *48*, 207−216.
(29) Cusnir, R.; Jaccard, M.; Bailat, C.; Christl, M.; Steinmann, P.; Haldimann, M.; Bochud, F.; Froidevaux, P. Probing the kinetic parameters of plutonium−naturally occurring organic matter interactions in freshwaters using the diffusive gradients in thin films technique. *Environ. Sci. Technol.* **2016**, *50*, 5103−5110.
(30) André, C.; Choppin, G. R. Reduction of Pu(V) by humic acid. *Radiochim. Acta* **2000**, *88*, 613−618.
(31) Morrison, K. D.; Jiao, Y.; Kersting, A. B.; Zavarin, M. Reduction of plutonium(VI) to (V) by hydroxamate compounds at environmentally relevant pH. *Environ. Sci. Technol.* **2018**, *52*, 6448−6456.
(32) Lin, P.; Xu, C.; Zhang, S.; Fujitake, N.; Kaplan, D. I.; Yeager, C. M.; Sugiyama, Y.; Schwehr, K. A.; Santschi, P. H. Plutonium partitioning behavior to humic acids from widely varying soils is related to carboxyl-containing organic compounds. *Environ. Sci. Technol.* **2017**, *51*, 11742−11751.
(33) Santschi, P. H.; Roberts, K. A.; Guo, L. Organic nature of colloidal actinides transported in surface water environments. *Environ. Sci. Technol.* **2002**, *36*, 3711−3719.
(34) Matkar, V. M.; Narayanan, U.; Bhat, I. S.; Pillai, K. C. Geochemical association of plutonium in sediments of the Trombay coastal environment. *J. Radioanal. Nucl. Chem.* **1992**, *156*, 119−127.
(35) Schwertmann, U. Inhibitory effect of soil organic matter on the crystallization of amorphous ferric hydroxide. *Nature* **1966**, *212*, 645−646.
(36) Riedel, T.; Zak, D.; Biester, H.; Dittmar, T. Iron traps terrestrially derived dissolved organic matter at redox interfaces. *Proc. Natl. Acad. Sci. U. S. A* **2013**, *110*, 10101−10105.
(37) Chen, C.; Dynes, J. J.; Wang, J.; Sparks, D. L. Properties of Fe-organic matter associations via coprecipitation versus adsorption. *Environ. Sci. Technol.* **2014**, *48*, 13751−13759.
(38) Tinnacher, R. M.; Begg, J. D.; Mason, H.; Ranville, J.; Powell, B. A.; Wong, J. C.; Kersting, A. B.; Zavarin, M. Effect of fulvic acid surface coatings on plutonium sorption and desorption kinetics on goethite. *Environ. Sci. Technol.* **2015**, *49*, 2776−2785.
(39) Lin, P.; Xu, C.; Kaplan, D. I.; Chen, H.; Yeager, C. M.; Xing, W.; Sun, L.; Schwehr, K. A.; Yamazaki, H.; Saito-Kokubu, Y. Nagasaki sediments reveal that long-term fate of plutonium is controlled by select organic matter moieties. *Sci. Total Environ.* **2019**, *678*, 409−418.
(40) Hatcher, O. S.; Schott, J. Iron colloids/organic matter associated transport of major and trace elements in small boreal rivers and their estuaries (NW Russia). *Chem. Geol.* **2002**, *190*, 141−179.
(41) Xu, C.; Athon, M.; Ho, Y.-F.; Chang, H.-S.; Zhang, S.; Kaplan, D. I.; Schwehr, K. A.; DiDonato, N.; Hatcher, P. G.; Santschi, P. H. Plutonium immobilization and remobilization by soil mineral and organic matter in the far-field of the Savannah River Site, US. *Environ. Sci. Technol.* **2014**, *48*, 3186−3195.
(42) Liao, P.; Li, W.; Jiang, Y.; Wu, J.; Yuan, S.; Fortner, J. D.; Giammar, D. E. Formation, aggregation, and deposition dynamics of NOM-iron colloids at anoxic-oxic interfaces. *Environ. Sci. Technol.* **2017**, *51*, 12235−12245.
(43) Zhang, P.; Yuan, S. Production of hydroxyl radicals from abiotic oxidation of pyrite by oxygen under circumneutral conditions in the presence of low-molecular-weight organic acids. *Geochim. Cosmochim. Acta* **2017**, *218*, 153−166.
(44) Page, S. E.; Kling, G. W.; Sander, M.; Harrold, K. H.; Logan, J. R.; McNeill, K.; Cory, R. M. Dark formation of hydroxyl radical in arctic soil and surface waters. *Environ. Sci. Technol.* **2013**, *47*, 12860−12867.
(45) Murphy, S. A.; Solomon, B. M.; Meng, S.; Copeland, J. M.; Shaw, T. J.; Ferry, J. L. Geochemical production of reactive oxygen species from biogeochemically reduced Fe. *Environ. Sci. Technol.* **2014**, *48*, 3815−3821.
(46) Tong, M.; Yuan, S.; Ma, S.; Jin, M.; Liu, D.; Cheng, D.; Liu, X.; Gan, Y.; Wang, Y. Production of abundant hydroxyl radicals from oxygenation of subsurface sediments. *Environ. Sci. Technol.* **2015**, *50*, 214−221.
(47) Waite, T.; Szymczak, R. Generation and decay of hydrogen peroxide in estuarine waters. *Mar. Freshwater Res.* **1988**, *39*, 289.
(48) Cooper, W. J.; Lean, D. R. S. Hydrogen peroxide concentration in a northern lake: photochemical formation and diel variability. *Environ. Sci. Technol.* **1989**, *23*, 1425−1428.
(49) Begg, J. D.; Zavarin, M.; Kersting, A. B. Plutonium desorption from mineral surfaces at environmental concentrations of hydrogen peroxide. *Environ. Sci. Technol.* **2014**, *48*, 6201−6210.

https://dx.doi.org/10.1021/acs.est.0c08195
Environ. Sci. Technol. 2021, 55, 1800−1810

(50) Pignatello, J. J.; Oliveros, E.; MacKay, A. Advanced oxidation processes for organic contaminant destruction based on the Fenton reaction and related chemistry. *Crit. Rev. Environ. Sci. Technol.* **2006**, *36*, 1−84.
(51) Paciolla, M. D.; Davies, G.; Jansen, S. A. Generation of hydroxyl radicals from metal-loaded humic acids. *Environ. Sci. Technol.* **1999**, *33*, 1814−1818.
(52) Molz, F.; Demirkanli, I.; Thompson, S.; Kaplan, D.; Powell, B. Plutonium transport in soil and plants: An interdisciplinary study motivated by lysimeter experiments at the Savannah River site. *Dynamics of Fluids and Transport in Complex Fractured-Porous Systems*; AGU and Wiley: Washington, DC, 2015.
(53) Tanaka, T. Functional groups and reactivity of size-fractionated Aldrich humic acid. *Thermochim. Acta* **2012**, *532*, 60−64.
(54) Powell, B. A.; Dai, Z.; Zavarin, M.; Zhao, P.; Kersting, A. B. Stabilization of plutonium nano-colloids by epitaxial distortion on mineral surfaces. *Environ. Sci. Technol.* **2011**, *45*, 2698−2703.
(55) Felmy, A. R.; Moore, D. A.; Rosso, K. M.; Qafoku, O.; Rai, D.; Buck, E. C.; Ilton, E. S. Heterogeneous reduction of PuO2 with Fe(II): Importance of the Fe(III) reaction product. *Environ. Sci. Technol.* **2011**, *45*, 3952−3958.
(56) Bertrand, P.; Choppin, G. Separation of actinides in different oxidation states by solvent extraction. *Radiochim. Acta* **1982**, *31*, 135−138.
(57) Bader, H.; Sturzenegger, V.; Hoigné, J. Photometric method for the determination of low concentrations of hydrogen peroxide by the peroxidase catalyzed oxidation of N, N-diethyl-p-phenylenediamine (DPD). *Water Res.* **1988**, *22*, 1109−1115.
(58) Kobashi, A.; Choppin, G.; Morse, J. A study of techniques for separating plutonium in different oxidation states. *Radiochim. Acta* **1988**, *43*, 211−216.
(59) Marquardt, C. M.; Seibert, A.; Artinger, R.; Denecke, M. A.; Kuczewski, B.; Schild, D.; Fanghänel, T. The redox behaviour of plutonium in humic rich groundwater. *Radiochim. Acta* **2004**, *92*, 617−623.
(60) Jianxin, T.; Yaozhong, C.; Zhangji, L. A kinetic study of the reduction of plutonium with humic acid. *Radiochim. Acta* **1993**, *61*, 73−76.
(61) Bissey, L.; Smith, J.; Watts, R. Soil organic matter-hydrogen peroxide dynamics in the treatment of contaminated soils and groundwater using catalyzed H_2O_2 propagations (modified Fenton's reagent). *Water Res.* **2006**, *40*, 2477−2484.
(62) Wu, Y.; Zhou, S.; Qin, F.; Zheng, K.; Ye, X. Modeling the oxidation kinetics of Fenton's process on the degradation of humic acid. *J. Hazard. Mater.* **2010**, *179*, 533−539.
(63) Huling, S.; Arnold, R. G.; Sierka, R. A.; Miller, M. R. Influence of peat on Fenton oxidation. *Water Res.* **2001**, *35*, 1687−1694.
(64) Yeh, C. K.-J.; Kao, Y.-A.; Cheng, C.-P. Oxidation of chlorophenols in soil at natural pH by catalyzed hydrogen peroxide: the effect of soil organic matter. *Chemosphere* **2002**, *46*, 67−73.
(65) Vione, D.; Merlo, F.; Maurino, V.; Minero, C. Effect of humic acids on the Fenton degradation of phenol. *Environ. Chem. Lett.* **2004**, *2*, 129−133.
(66) Kochany, J.; Lipczynska-Kochany, E. Fenton reaction in the presence of humates. Treatment of highly contaminated wastewater at neutral pH. *Environ. Technol.* **2007**, *28*, 1007−1013.
(67) Lipczynska-Kochany, E.; Kochany, J. Effect of humic substances on the Fenton treatment of wastewater at acidic and neutral pH. *Chemosphere* **2008**, *73*, 745−750.
(68) Lindsey, M. E.; Tarr, M. A. Inhibition of hydroxyl radical reaction with aromatics by dissolved natural organic matter. *Environ. Sci. Technol.* **2000**, *34*, 444−449.
(69) Miller, C. J.; Rose, A. L.; Waite, T. D. Impact of natural organic matter on H_2O_2-mediated oxidation of Fe(II) in a simulated freshwater system. *Geochim. Cosmochim. Acta* **2009**, *73*, 2758−2768.
(70) Miller, C. J.; Rose, A. L.; Waite, T. D. Hydroxyl radical production by H_2O_2-mediated oxidation of Fe(II) complexed by Suwannee River fulvic acid under circumneutral freshwater conditions. *Environ. Sci. Technol.* **2013**, *47*, 829−835.
(71) Duesterberg, C. K.; Waite, T. D. Process optimization of Fenton oxidation using kinetic modeling. *Environ. Sci. Technol.* **2006**, *40*, 4189−4195.
(72) Georgi, A.; Schierz, A.; Trommler, U.; Horwitz, C. P.; Collins, T. J.; Kopinke, F.-D. Humic acid modified Fenton reagent for enhancement of the working pH range. *Appl. Catal., B* **2007**, *72*, 26−36.
(73) Wang, F.; Wu, Y.; Gao, Y.; Li, H.; Chen, Z. Effect of humic acid, oxalate and phosphate on Fenton-like oxidation of microcystin-LR by nanoscale zero-valent iron. *Sep. Purif. Technol.* **2016**, *170*, 337−343.
(74) Voelker, B. M.; Sulzberger, B. Effects of fulvic acid on Fe(II) oxidation by hydrogen peroxide. *Environ. Sci. Technol.* **1996**, *30*, 1106−1114.
(75) Sanchez, A. L.; Murray, J. W.; Sibley, T. H. The adsorption of plutonium IV and V on goethite. *Geochim. Cosmochim. Acta* **1985**, *49*, 2297−2307.
(76) Buxton, G. V.; Greenstock, C. L.; Helman, W. P.; Ross, A. B. Critical review of rate constants for reactions of hydrated electrons, hydrogen atoms and hydroxyl radicals ·OH/·O^- in aqueous solution. *J. Phys. Chem. Ref. Data* **1988**, *17*, 513−886.
(77) Zou, J.; Ma, J.; Chen, L.; Li, X.; Guan, Y.; Xie, P.; Pan, C. Rapid acceleration of ferrous iron/peroxymonosulfate oxidation of organic pollutants by promoting Fe(III)/Fe(II) cycle with hydroxylamine. *Environ. Sci. Technol.* **2013**, *47*, 11685−11691.
(78) Hug, S. J.; Leupin, O. Iron-catalyzed oxidation of arsenic(III) by oxygen and by hydrogen peroxide: pH-dependent formation of oxidants in the Fenton reaction. *Environ. Sci. Technol.* **2003**, *37*, 2734−2742.
(79) Pang, S.-Y.; Jiang, J.; Ma, J. Oxidation of sulfoxides and arsenic(III) in corrosion of nanoscale zero valent iron by oxygen: evidence against ferryl ions (Fe(IV)) as active intermediates in Fenton reaction. *Environ. Sci. Technol.* **2011**, *45*, 307−312.
(80) Bataineh, H.; Pestovsky, O.; Bakac, A. pH-induced mechanistic changeover from hydroxyl radicals to iron(IV) in the Fenton reaction. *Chem. Sci.* **2012**, *3*, 1594−1599.
(81) Marsac, R.; Banik, N. L.; Marquardt, C. M.; Kratz, J. V. Stabilization of polynuclear plutonium(IV) species by humic acid. *Geochim. Cosmochim. Acta* **2014**, *131*, 290−300.
(82) Dardenne, K.; Seibert, A.; Denecke, M. A.; Marquardt, C. M. Plutonium (III, IV, VI) speciation in Gorleben groundwater using XAFS. *Radiochim. Acta* **2009**, *97*, 91−97.
(83) Catrouillet, C.; Davranche, M.; Dia, A.; Bouhnik-Le Coz, M.; Marsac, R.; Pourret, O.; Gruau, G. Geochemical modeling of Fe(II) binding to humic and fulvic acids. *Chem. Geol.* **2014**, *372*, 109−118.
(84) Spark, K. M.; Wells, J. D.; Johnson, B. B. The interaction of a humic acid with heavy metals. *Soil Res.* **1997**, *35*, 89−102.
(85) Powell, B. A.; Kaplan, D. I.; Serkiz, S. M.; Coates, J. T.; Fjeld, R. A. Pu(V) transport through Savannah River Site soils-an evaluation of a conceptual model of surface-mediated reduction to Pu(IV). *J. Environ. Radioact.* **2014**, *131*, 47−56.
(86) Nash, K.; Fried, S.; Friedman, A. M.; Sullivan, J. C. Redox behavior, complexing, and adsorption of hexavalent actinides by humic acid and selected clays. *Environ. Sci. Technol.* **1981**, *15*, 834−837.
(87) Sachs, S.; Schmeide, K.; Brendler, V.; Krepelová, A.; Mibus, J.; Geipel, G.; Heise, K.-H.; Bernhard, G. *Investigation of the Complexation and the Migration of Actinides and Non-radioactive Substances with Humic Acids under Geogenic Conditions: Complexation of Humic Acids with Actinides in the Oxidation State IV Th, U, Np*; final report; Hannover: Technische Informationsbibliothek, 2003.
(88) Marquardt, C.; Herrmann, G.; Trautmann, N. Complexation of neptunium(V) with humic acids at very low metal concentrations. *Radiochim. Acta* **1996**, *73*, 119−126.
(89) Seibig, S.; van Eldik, R. Kinetics of [FeII(edta)] oxidation by molecular oxygen revisited. New evidence for a multistep mechanism. *Inorg. Chem.* **1997**, *36*, 4115−4120.

https://dx.doi.org/10.1021/acs.est.0c08195
Environ. Sci. Technol. 2021, 55, 1800−1810

(90) Wang, G.; Hsieh, S.-T.; Hong, C.-S. Destruction of humic acid in water by UV light-catalyzed oxidation with hydrogen peroxide. *Water Res.* **2000**, *34*, 3882−3887.

https://dx.doi.org/10.1021/acs.est.0c08195
Environ. Sci. Technol. 2021, 55, 1800−1810